

OPEN

Paradigm shift in aerosol chemical composition over regions downwind of China

Itsushi Uno^{1*}, Zhe Wang^{1,2*}, Syuichi Itahashi³, Keiya Yumimoto¹, Yuki Yamamura⁴, Ayako Yoshino⁵, Akinori Takami⁵, Masamitsu Hayasaki⁶ & Byung-Gon Kim⁷

A rapid decrease in PM_{2.5} concentrations in China has been observed in response to the enactment of strong emission control policies. From 2012 to 2017, total emissions of SO₂ and NO_x from China decreased by approximately 63% and 24%, respectively. Simultaneously, decreases in the PM_{2.5} concentration in Japan have been observed since 2014, and the proportion of stations that satisfy the PM_{2.5} environmental standard (daily, 35 µg/m³; annual average, 15 µg/m³) increased from 37.8% in fiscal year (FY) 2014 (April 2014 to March 2015) to 89.9% in FY 2017. However, the quantitative relationship between the PM_{2.5} improvement in China and the PM_{2.5} concentration in downwind regions is not well understood. Here, we (1) quantitatively evaluate the impacts of Chinese environmental improvements on downwind areas using source/receptor analysis with a chemical transport model, and (2) show that these rapid emissions reductions improved PM_{2.5} concentrations both in China and its downwind regions, but the difference between SO₂ and NO_x reduction rates led to greater production of nitrates (e.g., NH₄NO₃) due to a chemical imbalance in the ammonia–nitric acid–sulfuric acid–water system. Observations from a clean remote island in western Japan and numerical modeling confirmed this paradigm shift.

The long-range trans-boundary transport behavior of pollutants in East Asia is an important environmental issue due to frequent outflows of heavy pollution. Among pollutants, PM_{2.5} (particulate matter less than 2.5 µm in diameter) poses serious human health risks, including lung cancer, respiratory disease, and asthma, particularly over China and its downwind regions^{1–5}. Serious PM_{2.5} pollution has been observed in the northern China region since the early 2010s. To reduce this pollution, China has implemented active clean air policies in recent years (e.g., the Action Plan for Prevention and Control of Air Pollution, enacted in September 2013). These plans include the phasing out of outdated industrial capacity, small high-emission factories, and small coal-fired industrial boilers, as well as the strengthening of emission standards for power plants, industries, and vehicles, and the replacement of residential coal use with electricity and natural gas^{6,7}. These strong emission-reduction policies in China have led to a successful reduction in PM_{2.5} concentration (e.g., PM_{2.5} concentrations decreased from 102 µg/m³ in 2013 to 43 µg/m³ in 2019, as observed at the U.S. embassy in Beijing). Rapid reductions in SO₂ and NO_x emissions were also confirmed using environmental satellite data⁸ and bottom-up emissions inventory studies¹. MODIS AOD (aerosol optical depth) data revealed that there has been a consistent trend of year-to-year decreases in China and its downwind regions. The chemical composition of PM_{2.5} also changed significantly over China, with especially large decreases in levels of organic matter, mineral components, and sulfate aerosols⁹. Studies have suggested that emission control has a dominant effect on PM_{2.5} reduction compared to inter-annual meteorological variation^{10–12}. Further research using bottom-up emission inventory and numerical models revealed that different emission control measures contribute to reductions in PM_{2.5}^{6,13}. Meanwhile, recent studies have reported significant health benefits resulting from PM_{2.5} improvements in China^{14,15}.

¹Research Institute for Applied Mechanics, Kyushu University, Fukuoka, Japan. ²State Key Laboratory of Atmospheric Boundary Layer Physics and Atmospheric Chemistry (LAPC), Institute of Atmospheric Physics (IAP), Chinese Academy of Sciences (CAS), Beijing, China. ³Central Research Institute of Electric Power Industry, Abiko, Chiba, Japan. ⁴Fukuoka Institute of Health and Environmental Science, Dazaifu, Fukuoka, Japan. ⁵National Institute for Environmental Studies, Tsukuba, Ibaraki, Japan. ⁶Japan Automobile Research Institute, Tsukuba, Ibaraki, Japan. ⁷Gangneung-Wonju National University, Gangneung, Korea. *email: uno@riam.kyushu-u.ac.jp; wangzhe@riam.kyushu-u.ac.jp

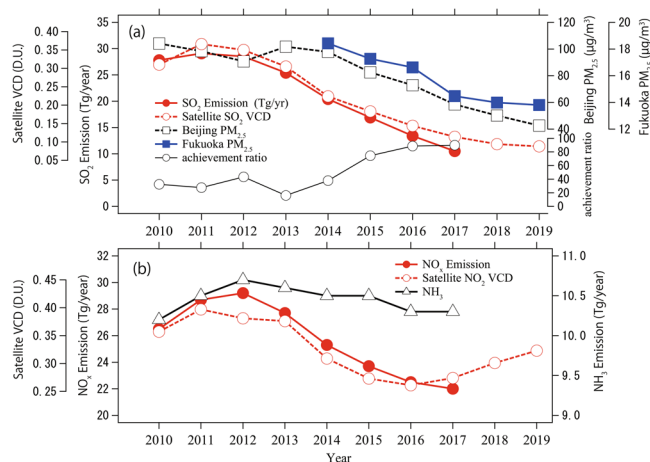


Figure 1. (a) Year-to-year trends of annually averaged PM_{2.5} concentrations at Beijing and Fukuoka, SO₂ emissions from China¹, vertical column densities of SO₂ over central eastern China (CEC) as calculated from OMI satellite data²⁴, and PM_{2.5} achievement ratios for Japan. (b) Year-to-year trends of NO_x and NH₃ emissions from China¹ and vertical column densities of NO₂ over CEC as calculated from OMI satellite data²⁴.

Focusing on regions downwind of China, the proportion of monitoring stations meeting the Japanese environmental standard for PM_{2.5} (defined as the achievement ratio) increased rapidly from 37.8% in fiscal year (FY) 2014 to 89.9% in FY 2017 (Ministry of Environment, Japan)¹⁶. During this period, Japanese pollutant emissions exhibited a slight decreasing trend¹⁷. Improvements in the PM_{2.5} achievement ratio result from complex interactions between Japanese and Chinese emission-reduction measures, and it is not yet clear which factor has a greater contribution. This lack of clarity arises because most PM_{2.5} studies are focused on an individual country, and quantitative evaluations or correlation analyses of the impacts of environmental improvement on downwind regions (beyond national borders) have rarely been published^{18–21}. Studying the relationship between decreased PM_{2.5} concentrations in China and its downwind regions and clarifying quantitative source/receptor (S/R) relationships are essential for establishing better environmental policies.

Remote island observations of aerosol chemical compositions off the west coast of Japan (eastern edge of the East China Sea) indicate that sulfate concentrations have decreased significantly, consistent with the decrease in SO₂ emissions in China. Although NO_x emissions also decreased, the observed nitrate concentration increased continuously in recent years²². This increase in the nitrate concentration could lead to excess N input to the oceans surrounding East Asia, which may have impacts on the marine ecosystem²³. In this paper, we support this observational finding with chemical transport model (CTM) sensitivity experiments, in which SO₂ and NO_x emissions are reduced at different rates to confirm the observed trend. These experiments showed that the observed nitrate increase can be explained by changes in the ammonia–nitric acid–sulfuric acid–water system balance due to the greater rate of decrease in SO₂ emissions compared to that in NO_x emissions.

Results

We analyzed hourly surface-level PM_{2.5} observational data from Japan and China and calculated the annual average PM_{2.5} concentration for each region. For Korea, we used annual average values from the Air Korea website. The observational data used in this study are described in the Methods section.

Satellite observations of NO₂ and SO₂ from the Ozone Monitoring Instrument (OMI) were also used for the analysis of emission trends between 2005 and 2019. Gridded (0.25 × 0.25 degree) Level 3 data from NASA were used for this study and annually-averaged data were used to examine year-to-year trends over China, Korea, and Japan (NASA OMI website)²⁴.

Figure 1 shows the annual average PM_{2.5} concentrations over Fukuoka, Japan and Beijing (at the U.S. Embassy), China (Supplementary Figure S1 shows the locations of the observation sites). This figure includes estimated SO₂, NO_x, and NH₃ emissions over China¹, and tropospheric vertical column densities (VCDs) of SO₂ and NO₂ over central eastern China (CEC) (OMI satellite data from 2011 to 2019)²⁴. This figure also shows the PM_{2.5} achievement ratio for Japan. Similar plots for the average of 74 cities in China and Korea (including two background sites), and several remote Japanese sites are provided in Supplementary Figure S2. Supplementary Figure S3 shows the annual average VCDs of SO₂ and NO₂ levels in East Asian regions between 2011 and 2019 based on satellite retrieval data. Supplementary Figure S4 shows the year-to-year average trends in three regions (CEC, Korea, and Japan) for SO₂ and NO₂ levels based on satellite observations.

The PM_{2.5} trends in Beijing and the average trend of 74 Chinese cities were very strongly correlated (Supplementary Figure S2(a)), although the PM_{2.5} concentration in Beijing was 40% higher than the average concentration of 74 cities in 2013 (this difference became negligible in 2018, as the rate of decrease in Beijing was greater). This trend was quite consistent with that in Japan (Supplementary Figure S2(c)). The correlation coefficient (R) between Beijing and Fukuoka was 0.98. The average PM_{2.5} trend for Korea (Supplementary Figure S2(b)) also showed a generally decreasing trend but with a slight difference from those in China and Japan up to 2017.

Bottom-up inventory results and satellite data also exhibit good correlations (Fig. 1). OMI SO₂ observations (Supplementary Figure S3) indicated that a rapid decrease in SO₂ was achieved over the CEC area, and the color

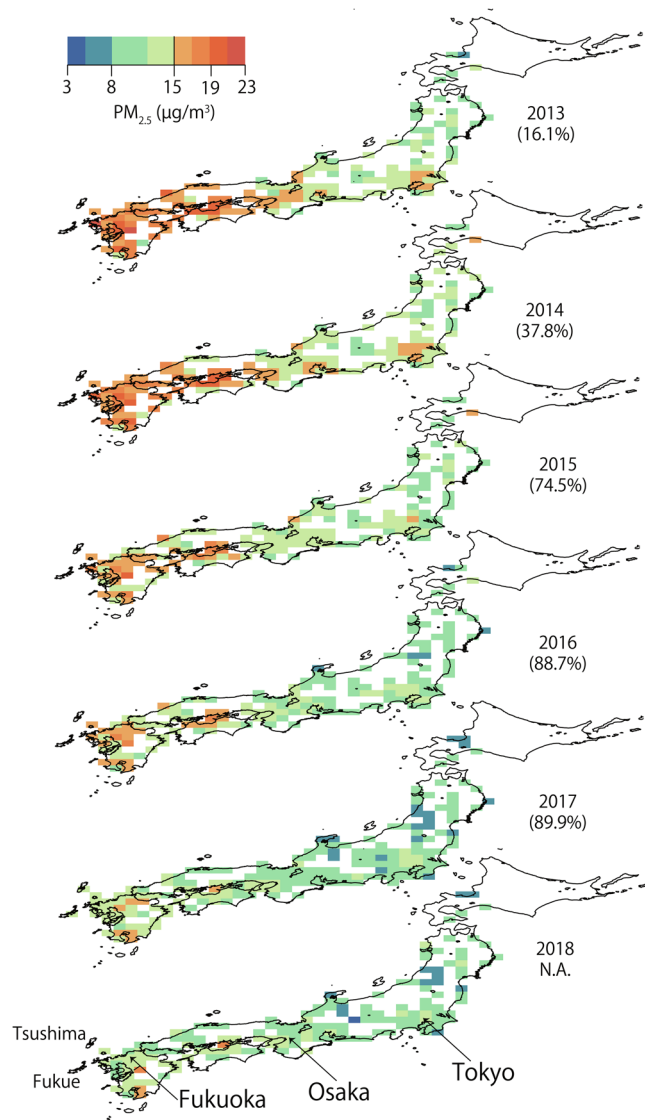


Figure 2. Horizontal distribution of annually averaged $PM_{2.5}$ concentrations over Japan between 2013 and 2018. Numbers in parentheses indicate $PM_{2.5}$ achievement ratios for Japan.

representing SO_2 in the image has been nearly absent since 2017 (using the same color scale). We found that the SO_2 VCDs in Korea and Japan exhibited small decreases or constant levels after 2010 (see Supplementary Figure S4), whereas NO_2 VCDs in Korea and Japan remained almost constant and increased slightly, respectively, since 2017. NO_2 VCDs exhibited an increasing trend over CEC after 2016.

Figure 2 shows the horizontal distribution of annually-averaged $PM_{2.5}$ in Japan from 2013 to 2018. The numbers in parentheses indicate the achievement ratios. $PM_{2.5}$ values were higher in the western part of Japan compared to the Tokyo metropolitan area. This pattern of high values in the west and low values in the east (i.e., a strong west-east gradient) indicates that the $PM_{2.5}$ concentration was strongly influenced by trans-boundary pollution from the west of Japan. From the year-to-year changes in $PM_{2.5}$, we found that the $PM_{2.5}$ concentration over large areas of Japan decreased rapidly from 2014 to 2015, with the achievement ratio increasing from 37.8% to 74.5% within one year. It is important to note that there was a high rate of decrease in $PM_{2.5}$ from 2014 to 2017, but the rate slowed down after 2017. This is because the recent decrease in the trans-boundary fraction is significant, and the improvement was dramatic and rapid across the rural/remote sites impacted by the trans-boundary fractions. The domestic emissions from large urban and industrial areas contribute greatly to the $PM_{2.5}$ concentration, at levels near or sometimes exceeding the criteria. In 2018, a few $PM_{2.5}$ hotspots could be observed in a very limited area with strong local effects from volcanoes and industrial emissions.

Figure 3 is similar to Fig. 2 but covers an extended region including Eastern China and Korea. Different colors in the figure represent different rates of decrease in observed $PM_{2.5}$ levels, defined as:

$$\Delta PM_{yyyy} = (PM_{2.5_2015} - PM_{2.5_yyyy}) / PM_{2.5_2015} \quad (1)$$

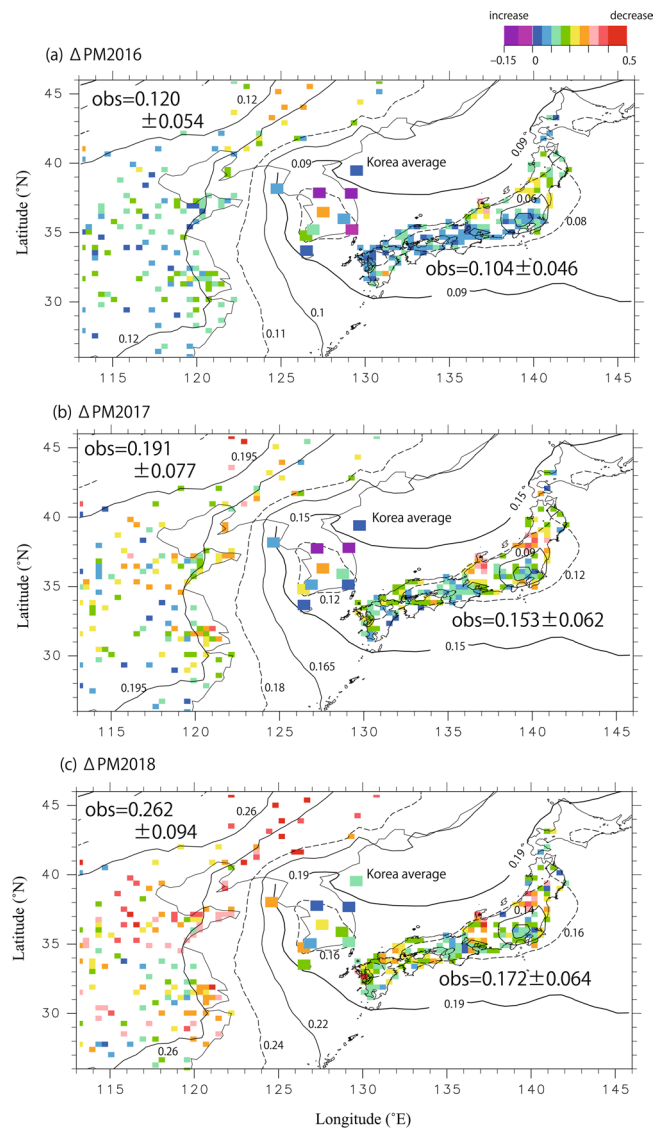


Figure 3. (a) Horizontal distribution of the rates of decrease in annually averaged $PM_{2.5}$ concentrations in 2016 compared with 2015 (see Eq. 1 for definitions). (b) Same as (a) but for 2017. (c) Same as (a) but for 2018. Note that the colored squares indicate observed rates of decrease in $PM_{2.5}$ concentrations, and contour lines represent rates of decrease over East Asia in response to different rates of decrease in $PM_{2.5}$ concentrations over China, as estimated from the simulated source-receptor (S/R) relationship.

where yyyy indicates a year. The rate was scaled based on the concentration in 2015. Negative values of ΔPM_{yyyy} indicate that $PM_{2.5}$ increased relative to 2015, as seen at some Korean sites. The annual average ΔPM_{yyyy} values over Eastern China (regionally averaged over 115°–123° E, 28°–43° N) from 2016 to 2018 were 0.120 ± 0.054 , 0.191 ± 0.077 , and 0.262 ± 0.094 , respectively. This result indicates that the observed average $PM_{2.5}$ concentration over Eastern China decreased by approximately 7% annually between 2016 and 2018.

The detailed changes over Japan were discussed in the context of Fig. 2. Figure 3 shows observed annual average rates of decrease (regionally averaged over 130°–142° E, 33°–37° N) of 0.104 ± 0.046 , 0.151 ± 0.062 , and 0.172 ± 0.064 since 2015. ΔPM_{yyyy} values for both the Korean average and individual stations are shown. A complicated variation in ΔPM_{yyyy} was observed, with some stations exhibiting positive changes or different variation patterns between years, except at the upwind background stations in Baengyeongdo and Jeju, which will be discussed later.

We used the 3-D Goddard Earth Observing System chemical transport model (GEOS-Chem)²⁵ for emission sensitivity analysis, including that of the S/R relationship for $PM_{2.5}$. Details of the GEOS-Chem settings and S/R analysis are described in the Methods section.

The model results were analyzed to obtain S/R values. We confirmed that the annual average contribution of Japanese domestic emissions to Fukuoka $PM_{2.5}$ was approximately 20%, and the Chinese contribution was approximately 60% based on the meteorological conditions in 2014²⁶. S/R results are very useful for evaluating possible strategies for improving $PM_{2.5}$ levels over downwind regions after enacting appropriate emission controls

in one region. For example, the contribution of PM_{2.5} from China (mainly from northern China) to Fukuoka was approximately 60%, and thus if the PM_{2.5} concentration in China decreases by 40% (e.g., from 100 to 60 µg/m³ in Beijing between 2014 and 2017), the decrease in PM_{2.5} concentration in Fukuoka can be calculated as follows: 60% × 40% = 24% (assuming that all emissions except those from China remain constant). The observed decrease in PM_{2.5} concentration in Fukuoka (18.5 to 14.5 µg/m³) was 22%, which is in good agreement with the model-based S/R estimate.

The contour lines in Fig. 3 represent S/R responses and were calculated by multiplying the fraction of the PM_{2.5} contribution from China at each point by the rate of decrease in Chinese PM_{2.5} concentration. The contours in Fig. 3(a–c) represent rates of decrease over East Asia in response to different decreases in PM_{2.5} concentration in China. The rate of decrease in PM_{2.5} concentration in China was set to 12%, 19%, or 26% based on observations. The observed relationship between rates of decrease in China and Japan can be explained using these contour lines.

For Korea, trends at the upwind background sites of Baengyeongdo and Jeju showed a consistent decreasing signal, in agreement with the decrease based on the S/R relationship. However, trends at other Korean sites cannot be explained by the S/R contour lines, and some cities (e.g., Seoul) exhibited significant increases in PM_{2.5} concentrations in 2016 and 2017 compared with 2015 and large year-to-year variations.

OMI SO₂ and NO₂ variations across Korea cannot explain the observed changes in the PM_{2.5} concentration. In Korea, the SO₂ VCD exhibited a small decrease or no change after 2010, and the NO₂ VCD remained almost unchanged (see Supplementary Figure S4); thus, the trend of the average PM_{2.5} was not clearly correlated with the local emissions pattern (particularly in urban areas). Elucidating these patterns and their drivers in Korea is a subject for future research.

We examined recent PM_{2.5} and aerosol composition changes over a clean and remote island, Fukue Island, which is located at the western edge of the Japanese mainland and eastern edge of the East China Sea (see Supplementary Figure S1). Details of the observations from Fukue Island and comparison with the GEOS-Chem simulation can be found in the Methods section.

Figure 4 shows observation results from Fukue Island averaged between February and April. Figure 4(a) shows the aerosol composition ratios among chloride, NO₃⁻, SO₄²⁻, NH₄⁺, and organic aerosols. Figure 4(b) shows a scatter diagram of SO₄²⁻ and NO₃⁻ for each year.

As shown in Fig. 4(a), the observed sulfate concentration decreased significantly (by 40%) at Fukue Island. This result is consistent with the decrease in SO₂ emissions over China. Although NO_x and NH₃ emissions were also reduced, the observed nitrate concentrations increased continuously. This result could be explained by the chemical balance of the ammonia–nitric acid–sulfuric acid–water system. This thermodynamic equilibrium process is included in the GEOS-Chem simulation described in the Methods section, which allows for detailed studies on chemical balance. Due to the extremely low vapor pressure of sulfuric acid, sulfuric acid produced in the atmosphere consumes ammonia and is neutralized, forming ammonium sulfate aerosol. Then, the leftover ammonia, referred to as free ammonia, is available for the potential formation of ammonium nitrate. As a result, the reduction of sulfuric acid causes more free ammonia to be available, leading to the formation of more ammonium nitrate. Seinfeld and Pandis (2016)²⁷ indicates that about half of the decrease in concentration of (NH₄)₂SO₄ will be offset by the increase in NH₄NO₃. The relationship between the decrease in sulfate and increase in nitrate depends primarily on the concentrations of their precursors, relative humidity (RH), and temperature.

Although SO₂, NO_x, and NH₃ emissions over China have all been reduced, the decrease in NO_x is significantly smaller than that in SO₂, and the decrease in NH₃ is much smaller than that in either SO₂ or NO_x (see Fig. 1). If the increase in nitrate due to SO₂ reduction is larger than the nitrate decreases due to decreases in NO_x and NH₃ emissions, the overall effects of emission control will lead to increased nitrate concentration. These phenomena were actually observed on Fukue Island from 2012 to 2019 (as seen in Fig. 4b), where sulfate decreased by 1.7 µg/m³, while nitrate increased by 1.7 µg/m³, causing the NO₃⁻ concentration to increase by almost four-fold compared to the 2012–2014 period. A more detailed analysis of these phenomena based on the GEOS-Chem model is described below.

Discussion

To quantitatively analyze the increase in NO₃⁻, we modeled an additional four cases of sensitivity experiments, changing the SO₂ and NO_x emission intensities based on the bottom-up Multi-resolution Emission Inventory for China (MEIC)¹ results (Table 1). Emission reduction was applied only in the China region, and emissions in all other regions were the same as in the control experiment.

CNTL (S10N10) was the control experiment. Case S04N08 was designed based on the MEIC emission reduction rate and OMI satellite changes, and thus is suitable for examining recent emission changes. Case S07N09 was designed to examine the linearity of decreases in SO₂ (between the S10, S07, and S04 cases), and case S04N10 was designed to examine NO_x sensitivity under a constant SO₂ condition (with S04N08). In this sensitivity study, emissions of NH₃ and non-methane volatile organic compounds were the same as in CNTL.

The results of the modeled sensitivity experiments are shown in Fig. 4(c) for SO₄²⁻ and NO₃⁻ in CEC, the centers of the Yellow Sea and East China Sea, and Fukue Island (model results were averaged between February and April for consistency with observations). Note that Fig. 4(c) demonstrates the typical response of the ammonia–nitric acid–sulfuric acid–water system to the emission sensitivity shown in Table 1. Thus, the absolute concentration level is different from the ACSM observation, but the fundamental changes observed can be explained by the model emission sensitivity experiment.

As shown in Fig. 4(c), the sensitivity experiment between CNTL (=S10N10) and S04N10 for CEC showed decreased SO₄²⁻ (Δ SO₄²⁻ = -4.5 µg/m³) and increased NO₃⁻ (Δ NO₃⁻ = +2.2 µg/m³), consistent with the response discussed in the Results section. The series of sensitivity experiments (CNTL, S07N09 and S04N08) shows a nearly linear response between Δ SO₄²⁻ and Δ NO₃⁻ even with decreasing NO_x emission. The differing

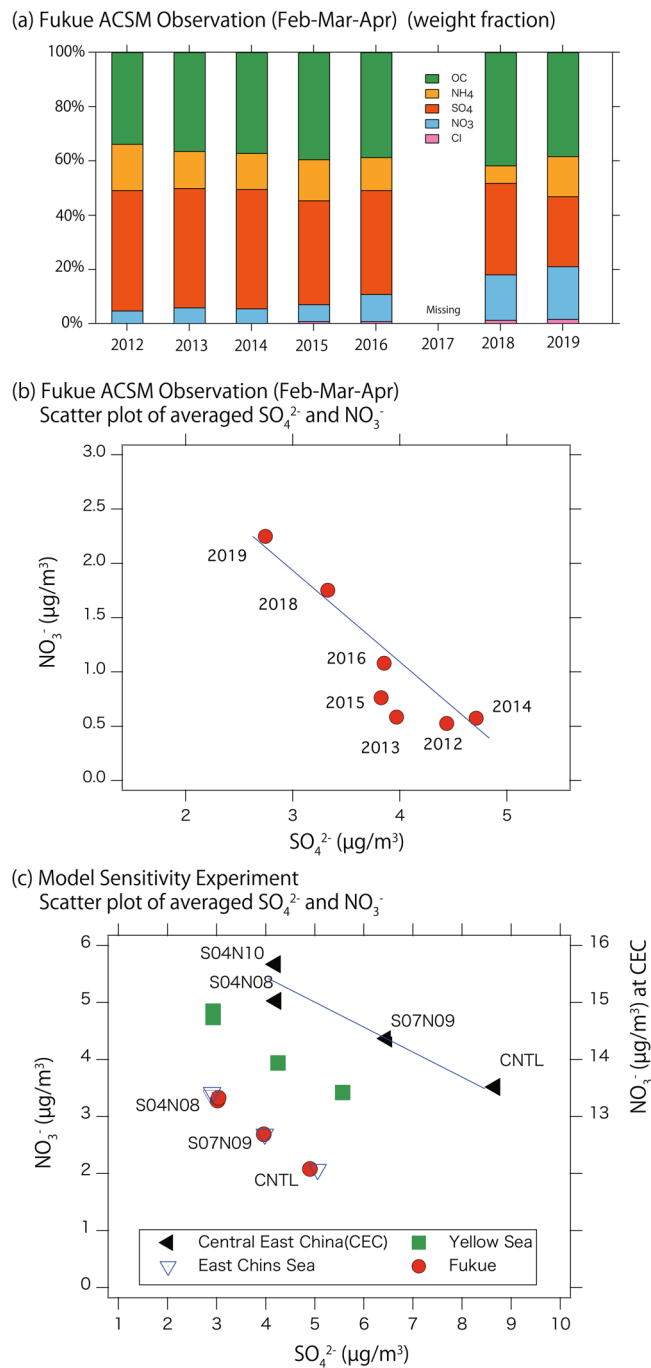


Figure 4. (a) Year-to-year changes in aerosol composition observed at Fukue Island (averaged from February to April), (b) scatter plot of averaged SO_4^{2-} and NO_3^- concentrations at Fukue Island from observation data and (c) GEOS Chem sensitivity analysis (extracted for CEC, Yellow Sea, East China Sea, and Fukue Island). Model results were averaged from February to April.

Case Code	Purpose	SO_2 emission	NO_x emission
CNTL (S10N10)	Control experiment	100%	100%
S04N08	Decrease relative to Fig. 1	40%	80%
S07N09	SO_2 linearity	70%	90%
S04N10	NO_x sensitivity	40%	100%

Table 1. Design of a model for sensitivity analysis of Chinese emissions.

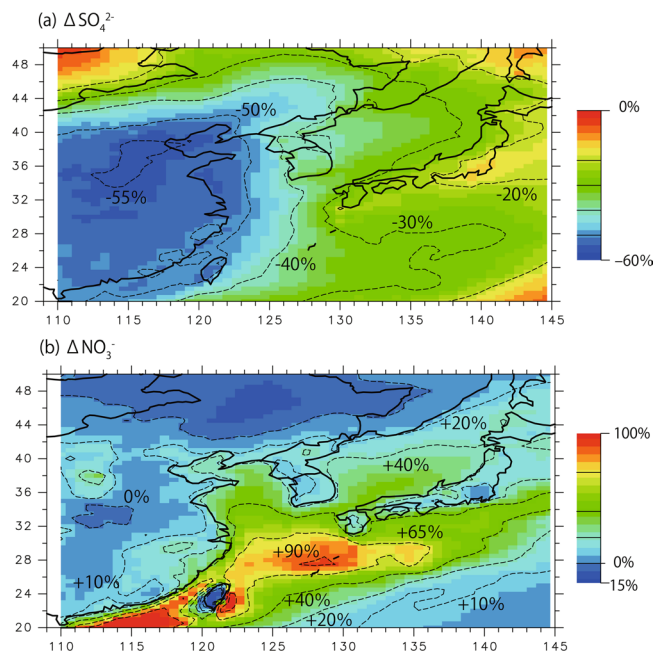


Figure 5. Horizontal distribution of relative changes in (a) SO_4^{2-} and (b) NO_3^- concentrations between the S04N08 sensitivity and CNTL cases based on annually averaged concentrations (see Eq. 2 for definitions).

responses of NO_3^- in S04N08 and S04N10 (NO_x emission difference) is most apparent for Beijing. This difference becomes very small over the downwind regions of the East China Sea and Fukue Island. The ratio of $\Delta\text{SO}_4^{2-} : \Delta\text{NO}_3^-$ ranges from 1:0.5 to 1:0.65, becoming larger as the transport distance increases. As noted above, the relationship between the decrease of sulfate and the increase of nitrate is strongly dependent on RH, temperature and a heterogeneous reaction with sea salt (for NaNO_3 formation) during transport from mainland China over the ocean. These responses are quite consistent with observations at Fukue Island.

The change in NH_3 concentration between CNTL and S04N08 is of great interest, and this result is shown in Supplementary Figure S5. The NH_3 concentration in the S04N08 experiment was more than double that over CEC (i.e., increase in free NH_3)²⁸, and NH_3 concentration increases were simulated over western Japan, including Fukue Island. The changes in NH_3 concentration over CEC were also supported by Infrared Atmospheric Sounding Interferometer (IASI) satellite observations²⁹. The conclusions of these sensitivity studies were reasonable, showing that reductions in SO_2 emissions change the balance of the ammonia–nitric acid–sulfuric acid–water system, creating free NH_3 that reacts with HNO_3 to form NH_4NO_3 , which is transported to downwind regions, especially in the cold season.

Figure 5 shows the horizontal distribution of scaled annual mean ΔSO_4^{2-} and ΔNO_3^- from the model sensitivity study, based on the CNTL and S04N08 experiments. These indices are calculated as follows:

$$\Delta\text{SO}_4^{2-} = (\text{SO}_4^{2-}_{\text{S04N08}} - \text{SO}_4^{2-}_{\text{CNTL}}) / \text{SO}_4^{2-}_{\text{CNTL}} \quad (2a)$$

$$\Delta\text{NO}_3^- = (\text{NO}_3^-_{\text{S04N08}} - \text{NO}_3^-_{\text{CNTL}}) / \text{NO}_3^-_{\text{CNTL}} \quad (2b)$$

The SO_4^{2-} decrease (ΔSO_4^{2-}) over mainland China exceeded -50% , consistent with the 60% decrease in SO_2 (Fig. 1a). Over western and eastern Japan, SO_4^{2-} decreased by 30% and 20% , respectively. We found that this rate of decrease was linearly proportional to the SO_2 reduction rate within China via a comparison with case S07N09. The impacts of the decrease in SO_2 in China clearly covered a large area downwind.

For NO_3^- , ΔNO_3^- over China was not significant, which is consistent with recent observations⁹. Several areas downwind of China exhibited increased NO_3^- . Over the East China Sea, the rate of increase in NO_3^- exceeded 90% , as NO_3^- concentrations were low in this area in the CNTL experiment; thus, a small increase in NO_3^- results in a large rate of increase. In the Fukue Island region, this increase was approximately 60% . Figure 5 shows annually averaged values, and ratios increased when averaged over the cold season (February to April) because NH_4NO_3 is more stable in cold weather, as discussed below.

Figure 6 shows time–longitude trends of the NO_3^- increase from experiments CNTL to S04N08 along the latitude of 32.5°N . This latitude corresponds the typical transport route from Shanghai to Fukue Island. The increase in concentrations over the downwind regions of China between December and March was significant and was caused by cold weather increasing NH_4NO_3 stability. During the warm season, the transport path changes and warm temperatures cause NH_4NO_3 aerosols to enter the gas phase as HNO_3 . At Fukue Island, the increase reached $1\mu\text{g}/\text{m}^3$ in winter, consistent in magnitude with observations at Fukue Island. Notably, the eastern edge of area in which NO_3^- increased (on the order of $0.5\mu\text{g}/\text{m}^3$) approaches 134°E to 136°E , where large cities such as Osaka are located. Note that the changes in concentration were small and usually difficult to detect from observations

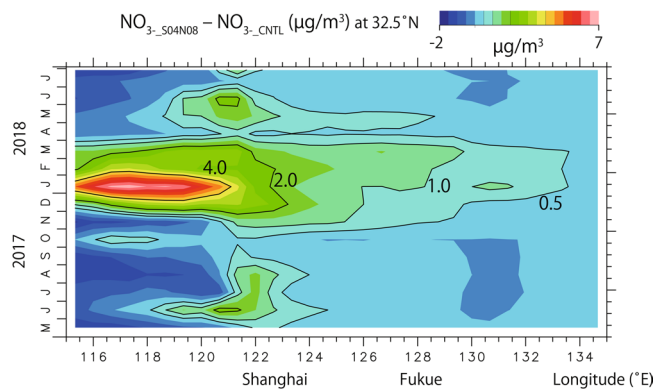


Figure 6. Time-longitude plot of the absolute concentration differences in NO_3^- (values of S04N08 sensitivity experiment – those of CNTL case) between March 2017 and July 2018 along the 32.5°N latitude line (model vertical level = 1).

over urban areas of mainland Japan due to large local NO_x emissions. However, this small increase may contribute significantly to the presence of excess nitrogen over the downwind region in East Asia²³.

Recent studies have described how a decrease in $\text{PM}_{2.5}$ can enhance the lifetime of OH radicals and increase the O_3 level³⁰ (followed by increases in the atmospheric oxidation capacity and NO_3^- formation). This is a reasonable mechanism that might increase the NO_3^- formation. However, our version of the GEOS-Chem model does not include the heterogeneous interaction between $\text{PM}_{2.5}$ and OH. Our results explain the observed $\text{SO}_4^{2-}/\text{NO}_3^-$ changes exactly, and this indicates that a change in the atmospheric oxidation capacity is not the primary reason for the observed changes in $\text{SO}_4^{2-}/\text{NO}_3^-$.

We analyzed the $\text{PM}_{2.5}$ observation data from 2014 to 2019 over Japan, Korea, and China, and found that there was a clear decreasing trend over Japan, which was strongly correlated with levels in China. An emission sensitivity study based on the GEOS-Chem chemical transport model was carried out to quantify the relationship between emission levels in China and $\text{PM}_{2.5}$ concentrations over downwind regions. The model results showed that the trend of an annual decrease in $\text{PM}_{2.5}$ in Japan was explained primarily by reduced $\text{PM}_{2.5}$ concentrations in China. We also used this model to quantitatively evaluate the impact of Chinese environmental improvements on downwind areas using S/R analysis. Rapid emission reductions played an important role in reducing $\text{PM}_{2.5}$ concentrations, but a chemical imbalance in the ammonia–nitric acid–sulfuric acid–water system caused an increase in long-range NO_3^- transport to downwind regions. Observations on a clean remote island and numerical modeling confirmed that this paradigm shift has occurred since 2014–2015. Concentrations of sulfate, a chemical that undergoes long-range transport, are decreasing, whereas those of nitrate, which is subject only to short-distance transport, are increasing. This increase in nitrate could lead to an excess nitrogen burden in East Asia and the surrounding oceanic regions^{31,32}. We found that the most recent satellite NO_2 and SO_2 VCDs, for 2019 (see Supplementary Figure S4), revealed that this paradigm shift is accelerating (because SO_2 is still decreasing, whereas NO_2 is now increasing), indicating that there is a need for careful continuous observation of changes in aerosol chemical compositions, both in China and the downwind regions of Japan and Korea.

Methods

Surface $\text{PM}_{2.5}$ observation data. For Japan, hourly $\text{PM}_{2.5}$ observation data from the Atmospheric Environmental Regional Observation System³³ (AEROS; also referred to as ‘Soramame-kun’) were used for calculating annually averaged $\text{PM}_{2.5}$ concentrations from 2013 to 2018. A total of 662 AEROS sites were used in this study, and after quality control processing, the AEROS data were interpolated into a 0.375° longitude–latitude grid. Data averaged across Japan were obtained from the Ministry of Environment of Japan.

For China, $\text{PM}_{2.5}$ concentration data were obtained from the China National Environmental Monitoring Center³⁴. In China, $\text{PM}_{2.5}$ concentrations have been monitored in 74 major cities since the end of 2012, including cities in the Beijing–Tianjin–Hebei region, Yangtze River Delta, and Pearl River Delta, as well as Chongqing municipalities and all provincial capitals. Data from these 74 cities were collected between 2013 and 2018, averaged, and used for analysis in this study. We also analyzed $\text{PM}_{2.5}$ observations taken at the U.S. Embassy in Beijing from 2011 to 2019.

For Korea, the annual average $\text{PM}_{2.5}$ values were obtained from the official Air Korea website of the Ministry of Environment of Korea³⁵. We selected nine sites, including the cities of Seoul, Busan, Gwangju, Gangneung, Daegu, Daejeon and Mokpo, as well as Jeju and the background site of Baengnyeongdo (the locations of the latter two sites are shown in Supplementary Figure S1) for analysis between 2015 and 2018. Data collected from multiple points within large cities were averaged.

We used observation sites with more than 250 days of qualified observations.

Chemical transport model and S/R analysis. We used the GEOS-Chem model for analysis²⁵. The model was run using the full GEOS-Chem NO_x - O_x - VOC - HO_x - CO chemistry option to simulate the formation of aerosols, including mineral dust, sea salt, black carbon (BC), organic carbon (OC), and secondary inorganic aerosols. The GEOS-Chem model used ISORROPIA-II³⁶ to calculate the detailed thermodynamic equilibrium

processes for the $\text{H}^+ - \text{NH}_4^+ - \text{K}^+ - \text{Ca}^{2+} - \text{Mg}^{2+} - \text{Na}^+ - \text{OH}^- - \text{SO}_4^{2-} - \text{NO}_3^- - \text{Cl}^- - \text{H}_2\text{O}$ aerosol system. The model used the assimilated meteorological fields from GEOS of the NASA Global Modeling and Assimilation Office. The model has a horizontal resolution of $2^\circ \times 2.5^\circ$ for global runs, and $0.5^\circ \times 0.667^\circ$ for Asian one-way nesting runs ($11^\circ \text{S} - 55^\circ \text{N}$, $70 - 150^\circ \text{E}$), both containing 47 vertical levels from the surface to 0.01 hPa. We used anthropogenic emissions data from the Emission Database for Global Atmospheric Research³⁷ for the global domain and from the Regional Emission Inventory in Asia (REAS; ver. 2.1) for the Asian domain³⁸. REAS NH_3 emissions data were modified to include seasonal variations in China³⁹. $\text{PM}_{2.5}$ concentrations from the model were calculated by summing the concentrations of relevant aerosols (BC, OC, SO_4^{2-} , NO_3^- , NH_4^+ , dust, and sea salt). Model simulation was conducted from the beginning of December 2013 to the end of July 2019, and the results from the first 8 months were used for model training. We primarily used the S/R model results for 2014 (when the pollution level was high) and assumed that the model results would be similar for the meteorology of different years. Other basic numerical settings were as reported in Uno *et al.*¹⁸. We set 19 source regions (including Japan, Korea, northern China, and central China) for S/R analysis²⁶. We used a 20% reduction of emission (not zero emission) to avoid undesirable non-linearity of the chemical reactions. The source contribution from region A is calculated as follows:

$$\text{Source contribution from region A} = (\text{PM}_{100, \text{all}} - \text{PM}_{80, \text{A}}) / (\text{PM}_{100, \text{all}} - \text{PM}_{80, \text{all}}),$$

where $\text{PM}_{100, \text{all}}$ is the $\text{PM}_{2.5}$ concentration under the 100% emission scenario for all regions.

Aerosol observations using the ACSM at Fukue Island. The chemical compositions and mass concentrations of atmospheric fine aerosols, i.e., fine particulate matter (PM_{1}), were observed at the remote island of Fukue, Nagasaki Prefecture, Japan (32.75°N , 128.68°E ; see Supplementary Figure S1). The population on this island is approximately 40,000 and it is generally considered to have few emission sources. Aerosol chemical composition was measured using a quadrupole-type ACSM (Q-ACSM; Aerodyne Research Inc., Billerica, MA, USA). The mass concentrations of $\text{PM}_{2.5}$ were obtained from an air-pollution monitoring station at Goto (located on Fukue Island), which is the site of municipal government offices for Nagasaki prefecture. The chemical compositions of ammonium, nitrate, sulfate, chloride, and organic compounds were analyzed. Because our main interest was trans-boundary air pollution from mainland China, measurements were taken only from January to May on Fukue Island. The details of Q-ACSM and calibration procedures for Fukue Island have been described previously^{22,40,41}. To confirm the model simulation, the ACSM observations and GEOS-Chem model results were compared over a 4-month period (Supplementary Figure S6). The GEOS-Chem experiment (CNTL) used emissions from 2010, and thus SO_4^{2-} and NO_3^- concentrations from GOES-Chem were over- and underestimated, respectively, but we confirmed that the model results reproduce the observed variations well.

Data availability

The datasets generated for the present study are available from the corresponding authors upon reasonable request.

Received: 16 January 2020; Accepted: 1 April 2020;

Published online: 15 April 2020

References

- Zheng, B. *et al.* Trends in China's anthropogenic emissions since 2010 as the consequence of clean air actions. *Atmospheric Chemistry and Physics* **18**, 14095–14111, <https://doi.org/10.5194/acp-18-14095-2018> (2018).
- Laden, F., Schwartz, J., Speizer, F. E. & Dockery, D. W. Reduction in fine particulate air pollution and mortality - Extended follow-up of the Harvard six cities study. *American Journal of Respiratory and Critical Care Medicine* **173**, 667–672 (2006).
- Tecer, L. H., Alagha, O., Karaca, F., Tuncel, G. & Eldes, N. Particulate matter ($\text{PM}_{2.5}$, $\text{PM}_{10-2.5}$, and PM_{10}) and children's hospital admissions for asthma and respiratory diseases: A bidirectional case-crossover study. *Journal of Toxicology and Environmental Health* **71**, 512–520 (2008).
- Burnett, R. T. *et al.* An integrated risk function for estimating the global burden of disease attributable to ambient fine particulate matter exposure. *Environmental Health Perspectives* **122**, 397–403 (2014).
- Cohen, A. J. *et al.* Estimates and 25-year trends of the global burden of disease attributable to ambient air pollution: an analysis of data from the Global Burden of Diseases Study 2015. *Lancet* **389**, 1907–1918 (2017).
- Zhang, Q. *et al.* Drivers of improved $\text{PM}_{2.5}$ air quality in China from 2013 to 2017. *Proceedings of the National Academy of Sciences* **116**, 24463–24469 (2019).
- Air Quality Policy Report—Tripartite Policy Dialogue on Air Pollution, <https://www.env.go.jp/press/files/jp/112834.pdf>.
- Itahashi *et al.* Inverse estimation of NO_x emissions over China and India 2005–2016: contrasting recent trends and future perspectives. *Environmental Research Letters* **14**, 124020 (2019).
- Wang, Y. *et al.* Trends in particulate matter and its chemical compositions in China from 2013–2017. *Science China Earth Sciences*, <https://doi.org/10.1007/s11430-018-9373-1> (2019).
- Zhai, S. *et al.* Fine particulate matter ($\text{PM}_{2.5}$) trends in China, 2013–2018: separating contributions from anthropogenic emissions and meteorology. *Atmospheric Chemistry and Physics* **19**, 11031–11041 (2019).
- Zhang, X. *et al.* The impact of meteorological changes from 2013 to 2017 on $\text{PM}_{2.5}$ mass reduction in key regions in China, Science China Earth Sciences, <https://doi.org/10.1007/s11430-019-9343-3> (2019).
- Dian, D. *et al.* Estimated contributions of emissions controls, meteorological factors, population growth, and changes in baseline mortality to reductions in ambient $\text{PM}_{2.5}$ and $\text{PM}_{2.5}$ -related mortality in China, 2013–2017. *Environmental Health Perspectives* **127**, 067009, <https://doi.org/10.1289/EHP4157> (2019).
- Cheng, J. *et al.* Dominant role of emission reduction in $\text{PM}_{2.5}$ air quality improvement in Beijing during 2013–2017: a model-based decomposition analysis. *Atmospheric Chemistry and Physics* **19**, 6125–6146 (2019).
- Zhang, J. *et al.* Cost-benefit analysis of China's Action Plan for Air Pollution Prevention and Control. *Frontiers of Engineering Management* **6**, 524–537 (2019).
- Zheng, Y. *et al.* Air quality improvements and health benefits from China's clean air action since 2013. *Environmental Research Letters* **12**, 114020 (2017).
- Ministry of Environment, Japan. <https://www.env.go.jp/press/106609.html>.

17. Ministry of Environment, Japan. <http://www.env.go.jp/air/osen/kotei/index.html>.
18. Uno, I. *et al.* Seasonal variation of fine- and coarse-mode nitrates and related aerosols over East Asia: synergetic observations and chemical transport model analysis. *Atmospheric Chemistry and Physics* **17**, 14181–14197 (2017).
19. Itahashi, S. *et al.* Nitrate transboundary heavy pollution over East Asia in winter. *Atmospheric Chemistry and Physics* **17**, 3823–3843 (2017).
20. Li, J. *et al.* A modeling study of source-receptor relationships in atmospheric particulate matter over Northeast Asia. *Atmospheric Environment* **91**, 40–51 (2014).
21. Kim, H. C. *et al.* Recent increase of surface particulate matter concentrations in the Seoul Metropolitan Area, Korea. *Scientific Reports* **7**, 4710 (2017).
22. Yoshino, A., *et al.* Analysis of aerosol chemical composition measured at urban and rural sites in Japan. Proceedings of the 20th International Conference on Nucleation and Atmospheric Aerosols, (Eds: R. Halonen, A. Nikandrova, J. Kontkanen, J. A. Enroth, H. Vehkamaeki), 566 (2017).
23. Taketani, F. *et al.* Seasonal response of north Pacific marine ecosystems to deposition of atmospheric inorganic nitrogen compounds from East Asia. *Scientific Reports* **8**, 9324 (2018).
24. NASA OMI web site: NO₂, https://disc.gsfc.nasa.gov/datasets/OMNO2d_V003/summary and SO₂, https://disc.gsfc.nasa.gov/datasets/OMS02e_V003/summary.
25. Bey, I. *et al.* Global modeling of tropospheric chemistry with assimilated meteorology: Model description and evaluation. *Journal of Geophysical Research* **106**, 73–95 (2001).
26. Uno, I., *et al.* Trans-boundary transport of PM_{2.5} to the western Japan and Japan Sea region based on source-receptor analysis, Earozou Kenkyu (Aerosol Research) **32**, 188–198 (in Japanese) (2017).
27. Seinfeld, J. H. & Pandis, S. N. *Atmospheric Chemistry and Physics - From air pollution to climate change* (3rd edition), Wiley (2016).
28. Liu, M. *et al.* Rapid SO₂ emission reductions significantly increase tropospheric ammonia concentrations over the North China Plain. *Atmospheric Chemistry and Physics* **18**, 17933–17943 (2018).
29. Lachatre, M. *et al.* The unintended consequence of SO₂ and NO₂ regulations over China: increase of ammonia levels and impact on PM_{2.5} concentrations. *Atmospheric Chemistry and Physics* **19**, 6701–6716 (2019).
30. Li, K. *et al.* A two-pollutant strategy for improving ozone and particulate air quality in China. *Nat. Geosci.* **12**, 906–910 (2019).
31. Itahashi, S., Hayami, H., Uno, I., Pan, X. & Uematsu, M. Importance of coarse-mode nitrate produced via sea salt as atmospheric input to East Asian oceans. *Geophysical Research Letters* **43**, 5483–5491 (2016).
32. Bleeker, A., Hicks, W. K., Dentener, F., Galloway, J. & Erisman, J. W. N deposition as a threat to the World's protected area under the Convention of Biological Diversity. *Environmental Pollution* **159**, 2280–2288 (2011).
33. <http://soramame.taiki.go.jp>.
34. China National Environmental Monitoring Center: <http://www.cnemc.cn>.
35. Air Korea: <http://www.airkorea.or.kr>.
36. Fountoukis, C. & Nenes, A. ISORROPIA II: A Computationally Efficient Thermodynamics Equilibrium Model for K⁺-Ca²⁺-Mg²⁺-NH₄⁺-Na⁺-SO₄²⁻-NO₃⁻-Cl-H₂O Aerosols. *Atmos. Chem. Phys.* **7**(17), 4639–4659 (2007).
37. Olivier, J. G. J. & Berdowski, J. J. M. Global emissions sources and sinks. In: Berdowski, J., Guicherit, R. and B.J. Heij (eds.) *The Climate System*, pp. 33–78. A.A. Balkema Publishers/Swets & Zeitlinger Publishers, Lisse, The Netherlands. ISBN 90 5809 255 0. (2001).
38. Kurokawa, J. *et al.* H. Emissions of air pollutants and greenhouse gases over Asian regions during 2000–2008: Regional emission inventory in Asia (REAS) version 2. *Atmospheric Chemistry and Physics* **13**, 11019–11058 (2013).
39. Huang, X. *et al.* A high-resolution ammonia emission inventory in China. *Global Biogeochemical Cycles* **26**, GB1030, <https://doi.org/10.1029/2011GB004161> (2012).
40. Ng, N. L. *et al.* An aerosol chemical speciation monitor (ACSM) for routine monitoring of the composition and mass concentrations of ambient aerosol. *Journal of Aerosol Science and Technology* **45**, 770–784 (2011).
41. Yoshino, A. *et al.* Influence of trans-boundary air pollution on the urban atmosphere in Fukuoka, Japan. *Atmosphere* **7**, 51 (2016).

Acknowledgements

This work was supported by MEXT/JSPS KAKENHI grant number JP18H03359 and the Environment Research and Technology Development Fund (5-1751, 2-1703, and 5-1951) of the Environmental Restoration and Conservation Agency of Japan.

Author contributions

I.U. designed the study. I.U., S.I. and Z.W. coordinated all analyses. A.Y. and A.T. conducted ACSM measurements and analyzed the data for Fukue Island. M.H. converted the AEROS PM_{2.5} data into gridded values. B.G.K. performed the data analysis for Korea. Y.Y. and K.Y. performed the overall data analysis. I.U. and Z.W. wrote the manuscript with valuable input from all coauthors.

Competing interests

The authors declare no competing interests.

Additional information

Supplementary information is available for this paper at <https://doi.org/10.1038/s41598-020-63592-6>.

Correspondence and requests for materials should be addressed to I.U. or Z.W.

Reprints and permissions information is available at www.nature.com/reprints.

Publisher's note Springer Nature remains neutral with regard to jurisdictional claims in published maps and institutional affiliations.



Open Access This article is licensed under a Creative Commons Attribution 4.0 International License, which permits use, sharing, adaptation, distribution and reproduction in any medium or format, as long as you give appropriate credit to the original author(s) and the source, provide a link to the Creative Commons license, and indicate if changes were made. The images or other third party material in this article are included in the article's Creative Commons license, unless indicated otherwise in a credit line to the material. If material is not included in the article's Creative Commons license and your intended use is not permitted by statutory regulation or exceeds the permitted use, you will need to obtain permission directly from the copyright holder. To view a copy of this license, visit <http://creativecommons.org/licenses/by/4.0/>.

© The Author(s) 2020